Surface Science 603 (2009) 3404–3409

Contents lists available at ScienceDirect

Surface Science

journal homepage: www.elsevier.com/locate/susc

Energetics of oxygen embedment into unreconstructed and reconstructed Cu(100) surfaces: Density functional theory calculations

Minyoung Lee, Alan J.H. McGaughey *

Department of Mechanical Engineering, Carnegie Mellon University, 5000 Forbes Avenue, Pittsburgh, PA 15213, United States

ARTICLE INFO

Article history:
Received 29 May 2009
Accepted for publication 2 October 2009
Available online 12 October 2009

Keywords:
Copper (100) surface
Copper oxidation
Oxygen embedment
Density functional theory
Nudged elastic band method

ABSTRACT

Atomic oxygen embedment into a Cu(100) surface is studied by density functional theory calculation and the nudged elastic band method. As the oxygen coverage increases on the unreconstructed surface from 0.25 monolayer (ML) to 0.75 ML, the energy barrier for oxygen embedment decreases and an energetically favorable sub-surface site is found at 0.75 ML coverage. At a fixed oxygen coverage of 0.5 ML, the oxygen embedment energetics vary with the surface morphology and the embedment is found to be more probable for reconstructed structures compared to the bare surface. On the missing-row reconstructed surface, we find that the energy barrier for atomic oxygen embedment is smaller through the missing-row compared to other paths, suggesting a mechanism for the formation of sub-surface oxygen structures that are consistent with a recent experiment. The energy barrier for sub-surface oxygen diffusion is predicted to be less than that for on-surface diffusion.

1. Introduction

Copper is a widely-studied and -used material, and it is important to understand how a copper surface interacts with its environment. For example, copper surfaces are being developed as efficient catalysts for the synthesis of bio-chemical compounds [1] and methanol for fuel cells [2].

When a copper surface is exposed to an oxygen environment, the oxygen molecules approach the surface, dissociate [3–6], and adsorb on the next–nearest–neighbor hollow sites [7]. As the surface-oxygen coverage approaches 0.5 monolayer (ML) on an initially clean Cu(100) surface, the surface structure transforms into the missing-row reconstruction [8–10] at temperatures lower than 473 K [11]. At temperatures between 473 and 1000 K, the $c(2\times2)$ with 0.25 ML disordered vacancy state and the (1×1) state with 1.0 ML coverage are experimentally observed [11]. It was traditionally believed that with further oxygen exposure, cuprite (Cu_2O) would grow as a uniform layer [12]. Yang and co-workers, however, found using transmission electron microscopy that Cu_2O islands nucleate and grow [13–17]. Thin film growth begins once the islands meet. The Cu_2O islands identified by Yang and co-workers grow into and out from the copper substrate as well as along it [16,17]. Lampimaki et al. later observed using scanning tunneling microscopy that individual missing-row reconstructions merge to form an ordered domain that is 1.8 Å higher than the clean surface and that Cu_2O islands form on these missing-row reconstructed domains [18]. Lampimaki et al. suggest that the elevated regions form as mobile copper adatoms stick to the phase boundaries between the missing-row reconstruction domains [18]. This explanation, however, is not sufficient to explain the subsequent oxide-island growth into the substrate, as it does not provide a mechanism for oxygen supply to the sub-surface region.

The shape of the Cu_2O islands, which grow by self assembly [19], depends on the oxidation temperature. An elongated nanorod structure is observed at 600 °C [14]. At higher temperatures, the oxide islands have pyramidal shapes [15]. To take advantage of the different oxide-island morphologies, which could be a source of components for nano-devices, a better understanding of the atomic-level mechanisms of copper oxidation is required.

Theoretical and modeling work has been performed on the oxygen-induced surface reconstruction and the early stages of the subsequent oxidation [3–6,20–28]. Alatalo and co-workers investigated oxygen adsorption [6] and the dynamics of oxygen dissociation and atomic adsorption [26] on the Cu(100) surface using density functional theory (DFT) calculations. Kangas et al. using DFT, calculated adsorption energies on the missing-row reconstructed Cu(100) surface for various amounts of on- and sub-surface oxygen coverage [25]. They found that the presence of sub-surface oxygen makes the system more energetically stable at 1.0 ML and higher oxygen coverages (including on- and sub-surface oxygen) [25]. Kangas and Laasonen found that oxygen embeds into the sub-surface more easily when there are adsorbed oxygen atoms both on the surface and in the sub-surface [28].

* Corresponding author.
E-mail address: mcgaughey@cmu.edu (A.J.H. McGaughey).

0039-6028/$ - see front matter © 2009 Elsevier B.V. All rights reserved.
doi:10.1016/j.susc.2009.10.002

The unit cell [$p\left(2\sqrt{2}\times\sqrt{2}\right)$] used in that study, however, was too small for the authors to determine if the missing-row plays an important role in the oxygen embedment.

The objective of this work is to apply DFT calculations to investigate oxygen embedding energetics and to identify potential embedding paths on the missing-row reconstructed Cu(100) surface. In Section 2, the computational unit cells, set-up, and procedures are presented. We investigate the relationship between the oxygen embedment energetics, surface oxygen coverage, and surface morphology in Sections 3.1 and 3.2. Then, we investigate the energetics of embedding an oxygen atom into the missing-row reconstruction along different embedding paths in Section 3.3. In Section 3.4, we examine how oxygen atoms diffuse between subsurface sites.

2. Calculation methodology

The Cu(100) surface morphologies used in this work are shown in Fig. 1. The oxygen coverage is defined as the fraction of face-centered cubic (fcc) hollow sites occupied by oxygen. To study the surface-oxygen coverage effect (Section 3.1), we use the $p(2\times2)$ and $p(4\times4)$ unit cells at 0.25, 0.5, 0.75, and 1.0 ML oxygen coverages. To study the surface morphology effect (Section 3.2), we use the $p\left(2\sqrt{2}\times2\sqrt{2}\right)$ unit cell at 0.5 ML coverage and three different surface morphologies [$c(2\times2)$, the missing-row reconstruction, and $c(2\times2)$ with 0.25 ML disordered vacancy]. The $c(2\times2)$ with 0.25 ML disordered vacancy morphology has one quarter of the first-layer copper atoms randomly replaced with vacancies [11]. For our DFT calculations, we obtain this structure by taking the missing-row reconstruction and moving one surface copper atom to the missing-row.

The DFT calculations are performed using the Vienna ab-initio simulation package (VASP) [29–33], which uses a plane-wave basis set [31,33]. We use ultra-soft pseudo potentials, the PW91 generalized gradient approximation [34], and apply a 330 eV energy cutoff.

The calculated bulk copper lattice constant is 3.65 Å, which is consistent with other DFT calculations [6,25,28]. The experimentally measured lattice constant is 3.61 Å [35]. The $p(2\times2)$ unit cell contains five copper layers, as shown in Fig. 2a and b. The $p(4\times4)$ unit cell contains four copper layers to decrease the computational load. For the $p\left(2\sqrt{2}\times2\sqrt{2}\right)$ unit cell, as shown in Fig. 2c and d, we use three copper layers due to the large number of atoms. The vacuum size is 11 Å for all cases. The bottom copper layer is fixed and the other layers are relaxed during the structure optimization. We found that a $p\left(2\sqrt{2}\times2\sqrt{2}\right)$ unit cell with five copper layers gave the same relaxed structure as that generated with three layers. The k-point mesh is generated by the Monkhorst–Pack scheme [36]. To be consistent with Kangas et al. [25], we use a $6\times6\times1$ mesh for the $p(2\times2)$ unit cell, a $3\times3\times1$ mesh for the $p(4\times4)$ unit cell, and an $8\times8\times1$ mesh for the $p\left(2\sqrt{2}\times2\sqrt{2}\right)$ unit cell. The $p\left(2\sqrt{2}\times2\sqrt{2}\right)$ unit cell is twice as big as that used by Kangas and co-workers [25,28]. This larger unit cell will allow us to investigate the energetics of embedding oxygen into the $c(2\times2)$ with 0.25 ML disordered vacancy structure (see Fig. 1) and through more paths.

To investigate the energetics of oxygen embedment into the copper surface, the climbing image nudged elastic band (NEB) method is applied [37–40]. The NEB method is a computational approach for finding the minimum energy path between specified initial and final equilibrium states. To specify the initial and final states, separate single-point DFT calculations are performed to ensure relaxed structures. We use spin-averaged calculations for the surface-adsorbed oxygen atoms and a dipole correction to compensate for having adsorbates on only one side of the structure. Based on the initial and final states, four images are created along the embedding path (see Fig. 2).

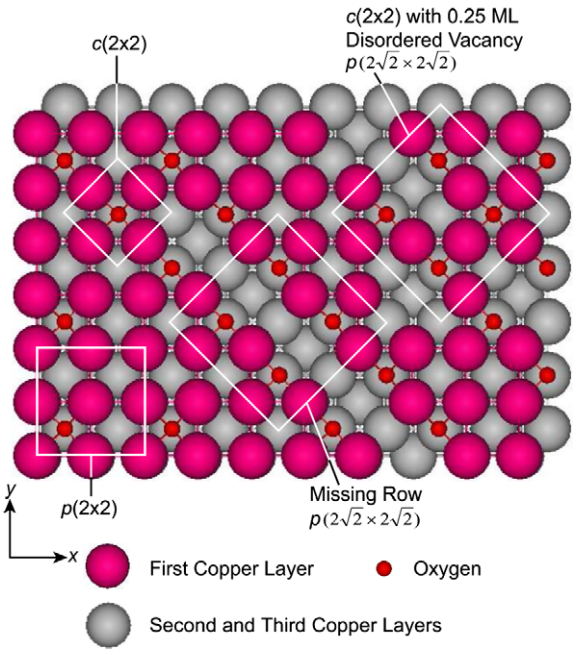

Fig. 1. Cu(100) surface structures used in this work. The squares indicate the unit cells. The $p(4\times4)$ unit cell area is four times bigger than the $p(2\times2)$ unit cell area.

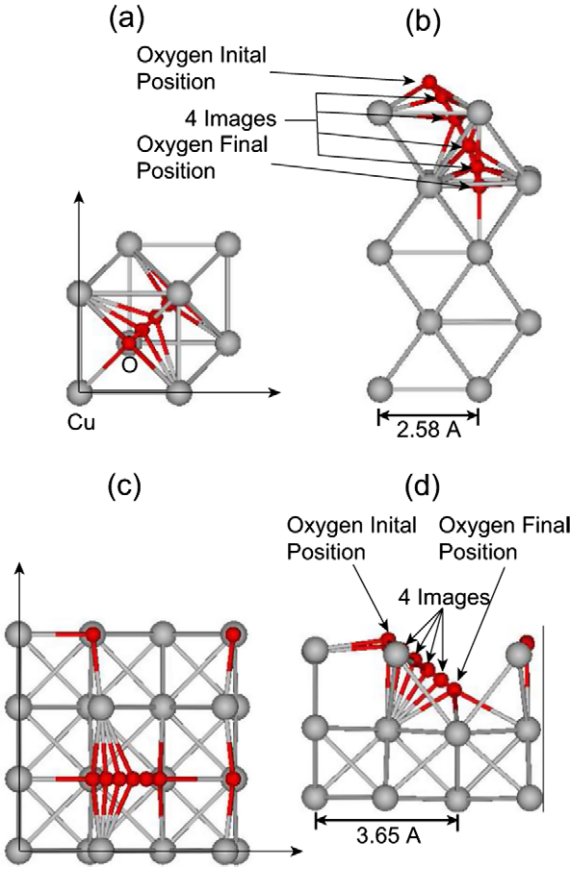

Fig. 2. (a) Top and (b) side view of the $p(2\times2)$ unit cell at 0.25 ML coverage with four images for a NEB calculation. (c) Top and (d) side view of the $p\left(2\sqrt{2}\times2\sqrt{2}\right)$ unit cell (missing-row reconstruction) at 0.5 ML coverage with four images for a NEB calculation.

The relative stabilities of the equilibrium structures are compared using the surface-oxide energy, E_S [41]:

$$E_S = \frac{E_{O/Cu} - N_{Cu} \cdot E_{Cu,bulk} - N_O \cdot \frac{E_{O_2}}{2}}{A_{surf}}. \quad (1)$$

Here, $E_{O/Cu}$ is the total system energy, $E_{Cu_{bulk}}$ is the energy of one atom in bulk fcc copper, and E_{O_2} is the energy of an isolated oxygen molecule. N_O and N_{Cu} are the total number of oxygen and copper atoms in the system, and A_{surf} is the unit-cell surface area. Because E_S is normalized by the unit-cell area, we can compare surfaces with different unit-cell sizes. A spin-polarized DFT calculation is used to obtain E_{O_2}.

We performed convergence tests for the $p\left(2\sqrt{2} \times 2\sqrt{2}\right)$ missing-row reconstructed surface for the number of k-points, the energy cutoff, and the number of copper layers. The total energy difference between $8 \times 8 \times 1$ and $12 \times 12 \times 1$ k-point meshes is 0.005 eV. The total energy difference between 330 and 600 eV energy cutoffs is 0.066 eV. The difference between $E_S \times A_{surf}$ for 3 layers and 8 layers is 0.048 eV. Based on these small energy changes, we believe that the energies reported in Section 3 are sufficiently converged to allow us to compare the different surfaces and oxygen embedment energetics.

3. Oxygen embedment energetics

3.1. Unreconstructed Cu(100) surface: role of oxygen coverage

In this section, we investigate the energetics of atomic oxygen embedment into the unreconstructed Cu(100) surface at 0.25, 0.5, 0.75 and 1.0 ML coverages. The 1.0 ML coverage corresponds to the experimentally observed (1×1) state [11]. In all calculations, there is only one embedding oxygen atom, which is initially located on the surface and then penetrates into the sub-surface site to the final state. The initial and final structures are both relaxed. For the 1.0 ML coverage final states, we find that there are two sub-surface oxygen atoms for the $p(2 \times 2)$ unit cell and a severe surface restructuring for the $p(4 \times 4)$ unit cell, which break the single oxygen atom embedment condition. Because of these findings, we do not report the embedding energetics for the 1.0 ML coverage.

In the initial state, all oxygen atoms are located on the on-surface fcc sites. As shown in Table 1, increasing the oxygen coverage makes the initial surface more stable for the lower coverages. At higher coverages, increased oxygen–oxygen repulsion leads to higher energies. In the final state, one oxygen atom is located in a sub-surface fcc site. Increasing the oxygen coverage makes the final state more energetically stable because the top copper layer hides the sub-surface oxygen atom, weakening the repulsive interactions between oxygen atoms [42]. The initial states are energetically more stable than the final states at 0.25 and 0.5 ML coverages. The final state is more stable than the initial state at 0.75 ML coverage, indicating that the oxygen embedment is energetically favorable. The trends for the $p(2 \times 2)$ and $p(4 \times 4)$ unit cells are comparable.

The NEB results are presented in Table 1 and Fig. 3a and b. In Table 1, the energy difference, E_{diff}, is calculated by subtracting the total system energy of the initial state from that of final state. The energy difference is positive at the lower oxygen coverages (0.25 and 0.5 ML) and negative at the higher coverage (0.75 ML). The negative value at higher coverage indicates that the sub-surface adsorption site is more stable than the on-surface site. The en-

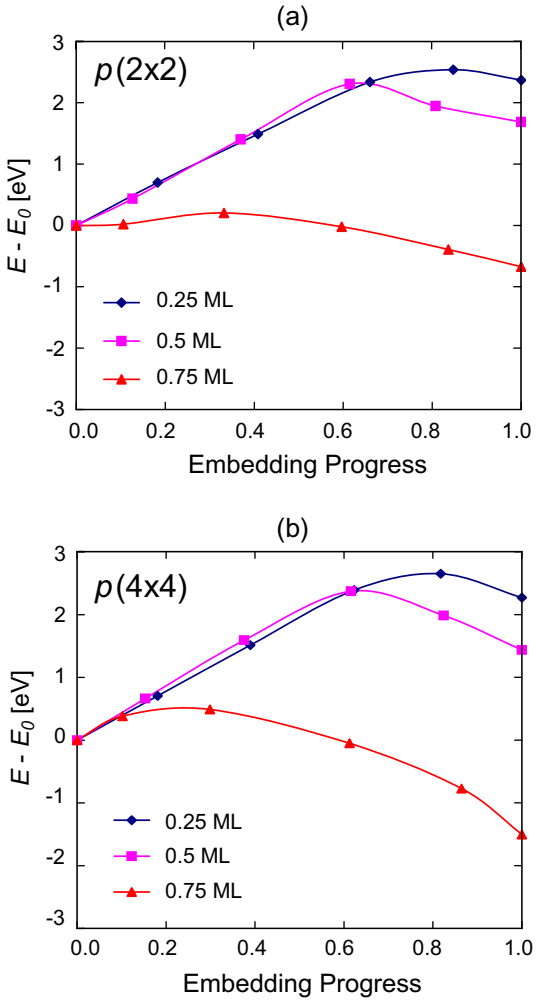

Fig. 3. Energetics of embedding an oxygen atom into the (a) the $p(2 \times 2)$ unit cell and (b) the $p(4 \times 4)$ unit cell (E = image energy, E_0 = energy of image 0). The embedding progress is the ratio of the embedding distance of each image to the total embedding distance. Lines are shown to guide the eye.

Table 1
Surface-oxide energy (E_S), energy difference (E_{diff}), and energy barrier ($E_{barrier}$) for oxygen embedment into the Cu(100) $p(2 \times 2)$ and $p(4 \times 4)$ unit cells at different oxygen coverages. The unit-cell area is 26.645 Å^2 for $p(2 \times 2)$ and 106.58 Å^2 for $p(4 \times 4)$. E_{diff} is calculated by subtracting the total system energy of the initial state from that of final state. $E_{barrier}$ is the energy difference between the initial state and the local energy maximum.

Coverage (ML)	Unit cell	$E_{S,Initial}$ (eV/Å^2)	$E_{S,Final}$ (eV/Å^2)	E_{diff} (eV)	$E_{barrier}$ (eV)
0.25	$p(2 \times 2)$	0.104	0.193	2.37	2.54
0.5	$p(2 \times 2)$	0.040	0.103	1.69	2.30
0.75	$p(2 \times 2)$	0.040	0.014	−0.67	0.20
1.0	$p(2 \times 2)$	0.062	–	–	–
0.25	$p(4 \times 4)$	0.106	0.128	2.27	2.65
0.5	$p(4 \times 4)$	0.042	0.055	1.44	2.37
0.75	$p(4 \times 4)$	0.040	0.026	−1.50	0.49
1.0	$p(4 \times 4)$	0.068	–	–	–

ergy barrier, $E_{barrier}$, is the energy difference between the initial state and the local energy maximum.

As the oxygen coverage increases, the energy barriers decrease for both the $p(2 \times 2)$ and $p(4 \times 4)$ unit cells. The energy barriers for the $p(4 \times 4)$ unit cell are slightly higher than these for the $p(2 \times 2)$ unit cell, but the trends are consistent. These results indicate that oxygen embedment will first occur between coverages of 0.5 and 0.75 ML, where the energy difference becomes negative and the energy barrier decreases.

3.2. Cu(100) surface at 0.5 ML coverage: role of surface morphology

In this section, we investigate the energetics of embedding an oxygen atom into surfaces with different morphologies. We use the same unit-cell size $[p(2\sqrt{2} \times 2\sqrt{2})]$ and oxygen coverage (0.5 ML) for all the calculations. For the different surface morphologies, we use (i) $c(2 \times 2)$, (ii) the missing-row reconstruction, and (iii) $c(2 \times 2)$ with 0.25 ML disordered vacancy. These structures are shown in Fig. 1. We choose the oxygen atom located in the lower-left position of the unit cell as the embedding oxygen atom for all morphologies (see Fig. 2c and d).

The embedding energetics are shown in Table 2 and Fig. 4. The energy differences are all positive, indicating that the initial state is more stable than the final state. The missing-row reconstruction and $c(2 \times 2)$ with 0.25 ML disordered vacancy structures have lower energy barriers than the $c(2 \times 2)$ surface. The energy barriers are all greater than 1 eV and embedment is thus not probable at 0.5 ML coverage [6,26,27]. Based on these findings, in the next section we will investigate the energetics of embedding an additional oxygen atom into the missing-row reconstructed surface.

Table 2
Surface-oxide energy (E_S), energy difference (E_{diff}), and energy barrier ($E_{barrier}$) for oxygen embedment into the Cu(100) $p(2\sqrt{2} \times 2\sqrt{2})$ unit cell with different surface morphologies ($c(2 \times 2)$w/0.25 DV is $c(2 \times 2)$ with 0.25 ML disordered vacancy). The unit-cell area is 53.290 Å^2 for all cases and the coverage is 0.5 ML.

Morphology	$E_{S,Initial}$ (eV/Å^2)	$E_{S,Final}$ (eV/Å^2)	E_{diff} (eV)	$E_{barrier}$ (eV)
$c(2 \times 2)$	0.049	0.078	1.55	1.96
Missing-row	0.039	0.066	1.43	1.55
$c(2 \times 2)$w/ 0.25 DV	0.043	0.062	1.02	1.43

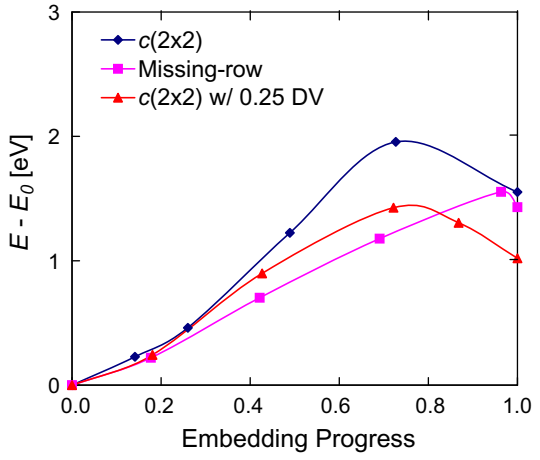

Fig. 4. Energetics of embedding an oxygen atom into the $p(2\sqrt{2} \times 2\sqrt{2})$ unit cell for different surface morphologies. (E = image energy, E_0 = energy of image 0) at 0.5 ML coverage. The embedding progress is the ratio of the embedding distance of each image to the total embedding distance. Lines are shown to guide the eye.

3.3. Reconstructed Cu(100) surface: role of embedding path

To identify potential oxygen embedding paths into the missing-row reconstruction, in this section we investigate atomic oxygen embedment into the $p(2\sqrt{2} \times 2\sqrt{2})$ unit cell. An oxygen coverage of 0.625 ML is considered, which includes one embedding oxygen atom and four surface-adsorbed oxygen atoms. The initial and final positions of the embedding oxygen atom (on-surface and sub-surface oxygen positions) are shown in Fig. 5a and b. All of these states are relaxed, stable structures. We adopt the notation of Kangas et al. [28]. "Hol", "tetra", and "octa" refer to the fcc hollow, tetrahedral, and octahedral sites. The energy difference (E_{diff}) and energy barrier ($E_{barrier}$) for six embedding paths are listed in Table 3 and the energetics are plotted in Figs. 6a and 7a.

As shown in Tables 1–3, the surface-oxide energies, E_S, for the missing-row reconstructed surfaces are smaller than those of the unreconstructed surface structures. This result indicates that the missing-row reconstructed surface is more stable than the other surfaces, consistent with a previous report [25].

Our objective is to determine how the embedment energetics differ between missing-row and non-missing-row paths. The missing-row paths are path1 (hol8 to octa4) and path3 (hol8 to octa2). The non-missing-row paths are path2 (hol7 to octa1) and path4 (hol7 to octa2). As shown in Fig. 6a and Table 3, the energy barrier is smaller through the missing-row paths (0.32 eV for path1 and 0.44 eV for path3) than through the non-missing-row paths (1.21 eV for path2 and 1.28 eV for path4). For comparison, the energy barrier predicted by DFT for the diffusion of an oxygen atom between hollow sites on a clean Cu(100) surface is 0.74 eV [6]. Oxygen embedment is thus more probable through the missing-

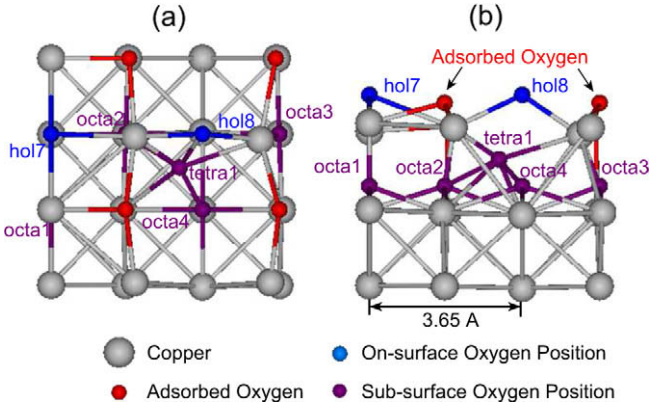

Fig. 5. (a) Top and (b) side view of the $p(2\sqrt{2} \times 2\sqrt{2})$ unit cell and the initial and final positions of the embedding oxygen atom.

Table 3
Surface-oxide energy (E_S), energy difference (E_{diff}), and energy barrier ($E_{barrier}$) for oxygen embedment into the missing-row reconstructed Cu(100) surface for different embedding paths. The initial and final positions of the embedding oxygen atom are shown in Fig. 5.

Index	Initial position	Final position	$E_{S,Initial}$ (eV/Å^2)	$E_{S,Final}$ (eV/Å^2)	E_{diff} (eV)	$E_{barrier}$ (eV)
path1 (mr)	hol8	octa4	0.034	0.031	−0.20	0.32
path2	hol7	octa1	0.026	0.031	0.27	1.21
path3 (mr)	hol8	octa2	0.034	0.030	−0.21	0.44
path4	hol7	octa2	0.026	0.030	0.22	1.28
path5(a)	octa4	tetra1	0.031	0.033	0.13	0.44
path5(b)	tetra1	octa2	0.033	0.030	−0.15	0.25
path6	octa2	octa1	0.030	0.031	0.05	0.70

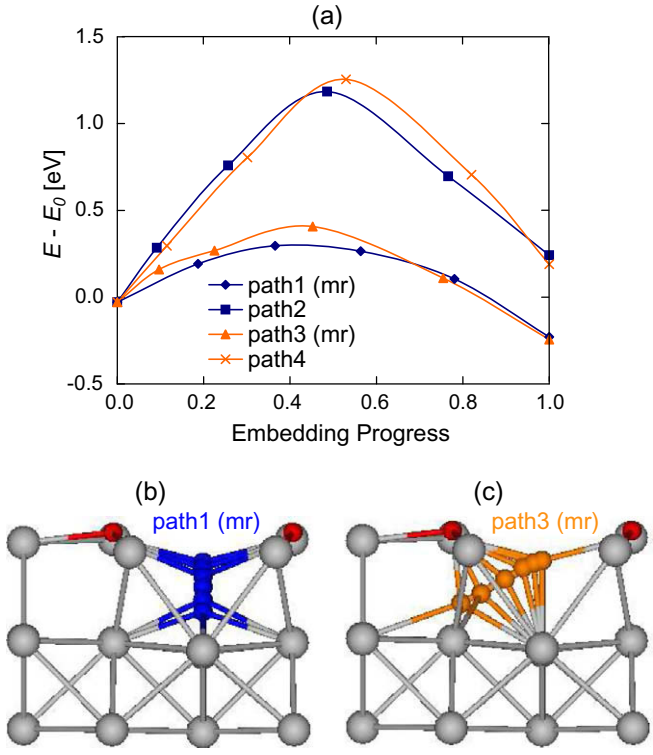

Fig. 6. (a) Embedding oxygen atom energetics for path1–path4 into the missing-row reconstructed Cu(100) surface. Illustrations for embedding (b) path1 and (c) path3. The initial and final positions of the embedding oxygen atom are provided in Table 3 and Fig. 5.

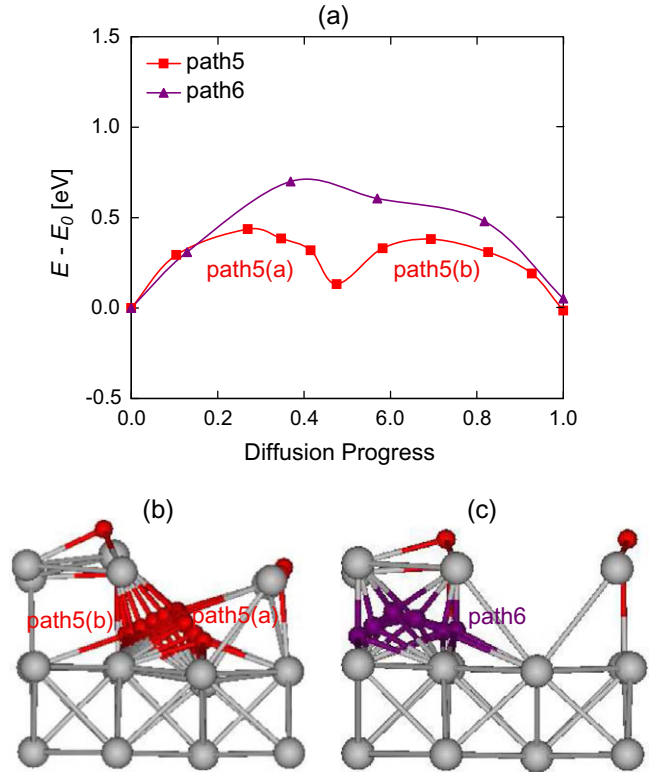

Fig. 7. (a) Sub-surface oxygen atom diffusion energetics for path5 and path6 in the missing-row reconstructed Cu(100) surface. Illustrations for embedding (b) path5 and (c) path6. The initial and final positions are provided in Table 3 and Fig. 5.

row. In addition, E_{diff} is negative only for the missing-row paths, indicating that the missing-row paths are energetically more favorable than non-missing-row paths.

3.4. Reconstructed Cu(100) surface: oxygen diffusion between sub-surface adsorption sites

As shown in Section 3.3, the energy barriers for oxygen embedment through the missing-row paths are smaller than that for surface diffusion. Previous DFT studies [25,28] found that when the missing-row reconstructed Cu(100) surface includes both on- and sub-surface oxygen adsorption, the surface is energetically more favorable than the case of only on-surface adsorption. Based on these two findings, we expect that oxygen atoms will diffuse between the sub-surface adsorption sites (octa1–octa4, see Fig. 5b). We investigate the sub-surface oxygen diffusion energetics by NEB calculation. The results are provided in Table 3 and Fig. 7a. We find that a local energy minimum exists between octa4 and octa2 (denoted by tetra1), and two seperate NEB calculations are thus performed. The energy barriers for path5 and path6 are smaller than or comparable to that for surface diffusion (0.74 eV), indicating that sub-surface diffusion is probable. This sub-surface diffusion mechanism may be useful in explaining how to form the on- and sub-surface adsorption structures suggested by previous DFT studies [25,28].

4. Conclusions

We have applied DFT calculations to study the energetics of embedding atomic oxygen into a copper surface. When the surface oxygen coverage increases on the unreconstructed Cu(100) surface, as shown in Fig. 3a and b, the energy barrier for the oxygen embedment decreases. The embedding energetics is found to vary with the surface morphology, with the reconstructed surfaces (missing-row reconstruction and $c(2\times2)$ with 0.25 ML disordered vacancy) being more favorable than the $c(2\times2)$ structure for oxygen embedment (see Fig. 4). As shown in Figs. 6a and 7a, on the missing-row reconstructed surface, the energy barriers for oxygen embedment through the missing-row and sub-surface diffusion are small compared to that for surface diffusion on a clean Cu(100) surface. These results indicate that oxygen embedment and sub-surface diffusion are potential mechanism for linking the missing-row reconstruction to Cu_2O island nucleation. Further experimental and computational work, however, is still required to test this hypothesis and to establish a clear path between the reconstructed surface and the bulk-like oxide.

Acknowledgements

This work is supported by the United States Department of Energy (Grant No. DOE FGOA01ER45919). We thank Prof. John Kitchin, Prof. Susan Sinnott, and Prof. Simon Phillipot for providing computational resources. We also thank Prof. Judith Yang and Dr. Dominic Alfonso for helpful discussions.

References

[1] L. Cecchi, F.D. Sarlo, F. Machetti, Chem. Eur. J. 14 (2008) 7903.
[2] W. Setthapun, S.K. Bej, L.T. Thompson, Top. Catal. 49 (2008) 73.
[3] T. Lederer, D. Arvanitis, G. Comelli, L. Troger, K. Baberschke, Phys. Rev. B 48 (1993) 15390.
[4] S. Liem, J. Clarke, G. Kresse, Surf. Sci. 459 (2000) 104.
[5] Y. Xu, M. Mavrikakis, Surf. Sci. 494 (2001) 131.
[6] M. Alatalo, S. Jaatinen, P. Salo, K. Laasonen, Phys. Rev. B 70 (2004) 2454171.
[7] T. Fujita, Y. Okawa, Y. Matsumoto, K. Tanaka, Phys. Rev. B 54 (1996) 2167.
[8] H.C. Zeng, R.A. McFarlane, K.A.R. Mitchell, Surf. Sci. 208 (1989) L7.
[9] F. Jensen, F. Besenbacher, E. Laegsgaard, I. Stensgaard, Phys. Rev. B 42 (1990) 9206.

[10] F.M. Leibsle, Surf. Sci. 337 (1995) 51.
[11] H. Iddir, D.D. Fong, P. Zapol, P.H. Fuoss, L.A. Curtiss, G. Zhou, J.A. Eastman, Phys. Rev. B 76 (2007). 241404(R)-1.
[12] N. Cabrera, N.F. Mott, Rep. Prog. Phys. 12 (1948) 163.
[13] J.C. Yang, B. Kolasa, J.M. Gibson, M. Yeadon, Appl. Phys. Lett. 73 (1998) 2841.
[14] G. Zhou, J.C. Yang, Phys. Rev. Lett. 89 (2002) 106101-1.
[15] G. Zhou, J.C. Yang, Appl. Surf. Sci. 210 (2003) 165.
[16] G. Zhou, J.C. Yang, Surf. Sci. 559 (2004) 100.
[17] G. Zhou, J.C. Yang, J. Mater. Res. 20 (2005) 1684.
[18] M. Lampimaki, K. Lahtonen, M. Hirsimaki, M. Valden, J. Chem. Phys. 126 (2007) 034703-1.
[19] G.M. Whitesides, M. Boncheva, PNAS 99 (2002) 4769.
[20] P.S. Bagus, F. Illas, Phys. Rev. B 42 (1990) 10852.
[21] H. Agren, V. Carravetta, L.G.M. Pettersson, Phys. Rev. B 53 (1996) 16074.
[22] J.R.B. Gomes, J.A.N.F. Gomes, Surf. Sci. 432 (2003) 279.
[23] S. Stolbov, A. Kara, T.S. Rahman, Phys. Rev. B 66 (2002) 245405-1.
[24] A. Puisto, H. Pitkanen, M. Alatalo, S. Jaatinen, P. Salo, A.S. Foster, T. Kangas, K. Laasonen, Catal. Today 100 (2005) 403.
[25] T. Kangas, K. Laasonen, A. Puisto, H. Pitkanen, M. Alatalo, Surf. Sci. 584 (2005) 62.
[26] M. Alatalo, A. Puisto, H. Pitkanen, A. Foster, K. Laasonen, Surf. Sci. 600 (2006) 1574.
[27] S. Jaatinen, J. Blomqvist, P. Salo, A. Puisto, M. Alatalo, M. Hirsimaki, M. Ahonen, M. Valden, Phys. Rev. B 74 (2007) 075402-1.
[28] T. Kangas, K. Laasonen, Surf. Sci. 602 (2008) 3239.
[29] G. Kresse, J. Hafner, Phys. Rev. B 47 (1993) 558.
[30] G. Kresse, J. Hafner, Phys. Rev. B 49 (1994) 14251.
[31] G. Kresse, J. Hafner, J. Phys.: Condens. Matter 6 (1994) 8245.
[32] G. Kresse, J. Furthmuller, Comput. Mater. Sci. 6 (1996) 15.
[33] G. Kresse, J. Furthmuller, Phys. Rev. B 54 (1996) 11169.
[34] J.P. Perdew, J.A. Chevary, S.H. Vosko, K.A. Jackson, M.R. Pederson, D.J. Singh, C. Fiolhais, Phys. Rev. B 46 (1992) 6671.
[35] N.W. Ashcroft, N.D. Mermin, Solid State Physics, Harcourt College Publishers, 1976.
[36] H.J. Monkhorst, J.D. Pack, Phys. Rev. B 13 (1976) 5188.
[37] H. Jonsson, G. Mills, K.W. Jacobsen, in: B.J. Berne, G. Ciccotti, D.F. Coker (Eds.), Classical and Quantum Dynamics in Condensed Phase Simulations, World Scientific, Singapore, 1998.
[38] G. Henkelman, B.P. Uberuaga, H. Jonsson, J. Chem. Phys. 113 (2000) 9901.
[39] G. Henkelman, H. Jonsson, J. Chem. Phys. 113 (2000) 9978.
[40] R.A. Olsen, G.J. Kroes, G. Henkelman, A. Arnaldsson, H. Jonsson, J. Chem. Phys. 121 (2004) 9776.
[41] I. Batyrev, A. Alavi, M.W. Finnis, Faraday Discuss. 144 (1999) 33.
[42] J.M. Hawkins, J.F. Weaver, A. Asthagiri, Phys. Rev. B 79 (2009) 125434-1.